Electronic Supplementary Material (ESI) for Catalysis Science & Technology.

Electronic Supplementary Information

Control of the single atoms/nanoparticles ratio in Pd/C catalysts to optimize the cooperative hydrogenation of alkenes

Authors: C. Rivera-Cárcamo, I. C. Gerber, I. del Rosal, B. Guicheret, R. Castro Contreras, L. Vanoye, A. Favre-Réguillon, B. F. Machado, J. Audevard, C. de Bellefon, R. Philippe and P. Serp

This file includes:

Materials and Methods

S.1 Materials

Carbon nanotube synthesis. A homemade $AlFeCoO_4$ catalyst was reduced in a fluidized bed reactor under a nitrogen (225 $mL \cdot min^{-1}$) and hydrogen (150 $mL \cdot min^{-1}$) flow at 650 °C. After the reduction step, the ethylene flow was adjusted to 225 $mL \cdot min^{-1}$ for 30 min to produce CNT. The CNT were recovered and then purified using an aqueous solution (50 vol% H_2SO_4) under reflux at 140 °C for 3 h. The acidic solution was then filtered and the solid washed with distilled water. The resulting solid was dried in an oven at 80 °C overnight. A portion of purified CNT was then functionalized with HNO_3 under reflux at 140 °C for 3 h. The acidic solution was filtered and washed with distilled water. The resulting solid was dried in an oven at 80 °C overnight to produce functionalized CNT (CNT). Another portion of purified CNT was treated in a horizontal tube oven under a nitrogen flow at 1000 °C for 1 h to produce high-temperature-treated CNT_{HT}.

Few Layer graphene synthesis. A homemade $CoFe_2O_4$ catalyst was reduced in a fluidized bed reactor under a nitrogen (225 $mL \cdot min^{-1}$) and hydrogen (150 $mL \cdot min^{-1}$) flow at 650 °C. After reduction step, the ethylene flow was adjusted to 225 $mL \cdot min^{-1}$ for 30 min to produce FLG. The FLG was recovered and purified at room temperature overnight using HCl. The acidic solution was then filtered and washed. The resulting solid was dried in an oven at 80 °C overnight. A portion of purified FLG was then functionalized with HNO_3 under reflux at 140 °C for 3 h. The acidic solution was filtered and washed. The resulting solid was dried in an oven at 80 °C overnight. Another portion of purified FLG was treated in a horizontal tube oven under a nitrogen flow at 1000 °C for 1 h to produce high-temperature-treated FLG (FLG_{HT}).

Carbon nanofiber synthesis. Carbon nanofibers were prepared using a 10%Ni/Al_2O_3 catalyst. The synthesis of the CNF was carried out in two steps: first, 2 g of 10%Ni/Al_2O_3 catalyst was reduced in a fluidized bed under a nitrogen (160 $mL \cdot min^{-1}$) and hydrogen (120 $mL \cdot min^{-1}$) flow at 650 °C; in the second step, the ethylene flow was adjusted to 60 $mL \cdot min^{-1}$ for 1 h. The CNF were recovered and purified using an aqueous solution (50 vol% H_2SO_4) under reflux at 80 °C for 3 h. The acidic solution was then filtered and washed. The resulting solid was dried in an oven at 80 °C overnight. A portion of purified CNF was then functionalized using HNO_3 under reflux at 80 °C for 3 h. The acidic solution was filtered and washed. The resulting solid was dried in an oven at 80 °C overnight. Another portion of the purified sCNF was then treated in a horizontal tube oven under a nitrogen flow at 1000 °C for 1 h to produce high-temperature-treated CNF (CNF_{HT}).

Palladium catalyst synthesis.

Supplementary Table 1. Catalysts properties.

Catalyst	Pd loading (%)	NP size from TEM (nm)[a)]	Pd dispersion (%)[c)]	SA/NP ratio[d)]
Pd/Al_2O_3	5	3.9 ± 1.1	31	n.d.[e)]
Pd/C	5	2.4 ± 1.0	46	n.d.[e)]
Pd/CNT also named **$Pd_{2\ SA/NP}$/CNT**	2	2.2 ± 1.1	49	2
$Pd_{2\ SA/NP}/CNT_{HT}$	1.6	2.2 ± 1.1	49	2
Pd_{SA}/CNT	0.1	-	-	no NP
$Pd_{1000\ SA/NP}$/CNT	0.1	1 ± 0.5[b)]	-	1000
$Pd_{200\ SA/NP}$/CNT	1.2	0.5 ± 0.1	-	200
$Pd_{60\ SA/NP}$/CNT	1.2	0.8 ± 0.3	-	60
$Pd_{40\ SA/NP}$/CNT	1.2	0.9 ± 0.3	-	40
$Pd_{10\ SA/NP}$/CNT	1.2	1.1 ± 0.6	-	10
Pd/FLG	1.9	2.6 ± 1.6	43	10
Pd/FLG_{HT}	1.7	2.5 ± 1.9	44	n.d.[e)]
Pd/CNF	1.7	1.5 ± 0.9	67	n.d.[e)]
Pd/CNF_{HT}	1.0	1.3 ± 1.1	76	n.d.[e)]

a) Calculated over 300 NP from STEM-HAADF micrographs

b) Calculated over 20 NP from STEM-HAADF micrographs

c) Metal dispersion was evaluated from a universal mathematical relation between the mean relative size of metallic crystallites and their dispersion [1].

d) SA/NP ratio in number calculated over 500 elements from STEM-HAADF micrographs.

e) n.d.: not determined

S.2 Catalytic experiments

H_2-assisted isomerization of 1-octene

Isomerization of alkenes was assessed using a dedicated experience. 1-octene was used as a molecular probe (see scheme below). The different isomers and by-product that could be obtained during the isomerization of 1-octene by Pd catalysts is shown below:

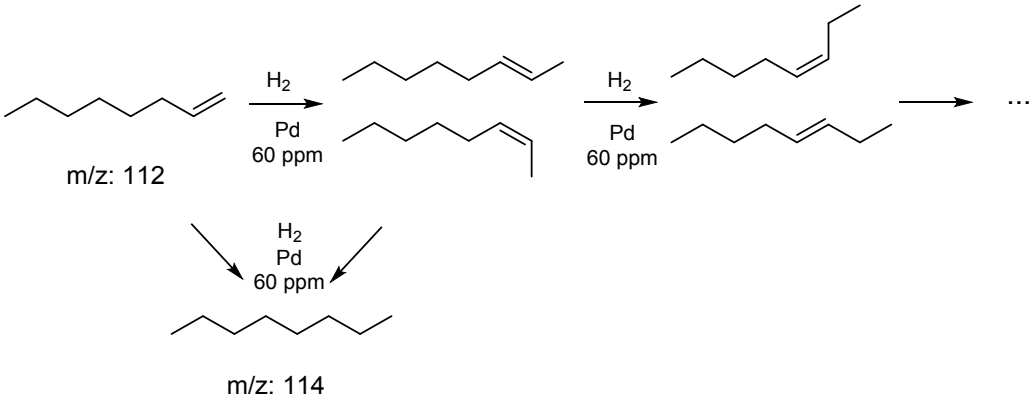

H_2-assisted isomerization of 1-octene

60 mL of a solution of 1-octene (Sigma Aldrich, 99%) in heptane (1 M) was added in a 100 mL round bottom flask and then heat at reflux under H_2 atmosphere. A sample was taken for *ex-situ* analysis and then catalyst was added in one portion. The mass of the catalyst was adjusted in order to have 3.75 µmol of Pd (0.4 mg, 60 ppm). Samples were taken as the function of time and were analyzed using GC-FID analysis.

The concentration of isomers of 1-octene and octane could be easily followed by GC as shown below.

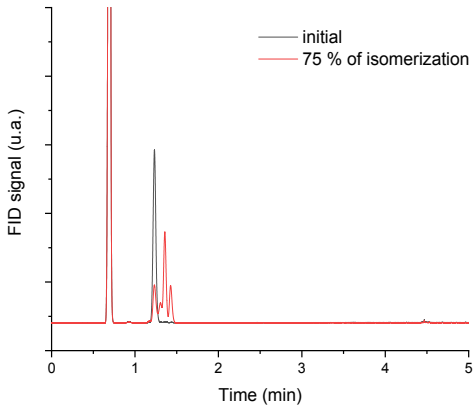

GC-FID of the reaction mixture

The absence of hydrogenation product (*i.e. n*-octane) was assessed by comparison with pure octane and by GC-MS analysis (see chromatogram below). Under those conditions, no hydrogenation product (*i.e.* n-octane) could be identified in the reaction mixture. This was

confirmed by comparison with pure octane and by GC-MS analysis in SIM mode (see chromatogram below).

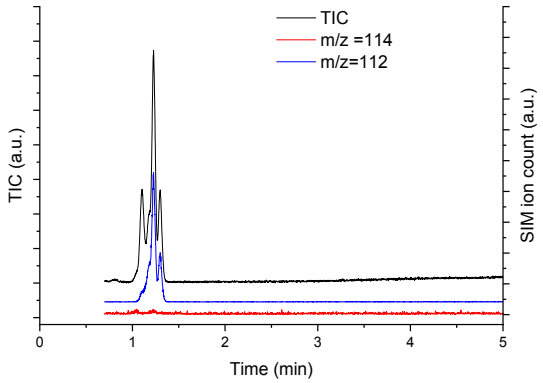

GC-MS chromatogram TIC and SIM ion count of a sample at 75 % of isomerization. Reaction conditions: 1 M 1-octene in heptane (1 M), reflux (98°C), H_2 1 atm.

The comparison of the 1-octene isomerization by the Pd catalysts is shown in Supplementary Fig. 7.

S.3 Assessment of the impact of mass transfer for myrcene hydrogenation

Mass transfer limitations have been evaluated using common chemical engineering approaches regarding the limiting reagent H_2. The physical properties of the different phases involved in the reaction are listed in the following Supplementary Table 2. Gas and liquid properties are given for 20 bar and 120 °C.

Supplementary Table 2: Physical properties of the different phases at 120 °C and 20 bar.

Phase	Name	Symbol	Value	Units
Liquid	Viscosity[a]	μ_L	1.71×10^{-4}	Pa.s
	Density	ρ_L	703	kg/m^3
	Surface tension[a]	σ_L	1×10^{-2}	N/m
	H_2 diffusivity[a]	$D_{m,H2}$	1.99×10^{-9}	m^2/s
	H_2 solubility[b]	C^*_{H2}	187	mol/m^3_L
Gas	Viscosity[a]	μ_G	1.07×10^{-5}	Pa.s
	Density	ρ_G	1.22	kg/m^3
CNT support	Skeleton density[c]	ρ_S	1900	$kg/m^3_{skeleton}$
	Pore volume[d]	V_{pore}	2.5	mL/g
	Dry particle density[d]	ρ_P	600	$kg/m^3_{particle}$
	Wetted particle density	ρ_p	1080	$kg/m^3_{particle}$
	Internal porosity[e]	β_P	70%	$m^3_{void}/m^3_{particle}$
	Tortuosity[f]	τ	≈1	-
	Mean Particle (agglomerate) diameter[4]	d_P	1-2	µm
γ-Al_2O_3 support	Skeleton density	ρ_S	3650	$kg/m^3_{skeleton}$
	Dry particle density	ρ_P	1460	$kg/m^3_{particle}$
	Wetted particle density	ρ_p	1880	$kg/m^3_{particle}$
	Internal porosity	β_P	60%	$m^3_{void}/m^3_{particle}$
	Tortuosity	τ	≈ 3	-
	Mean Particle diameter	d_P	25	µm
Activated Carbon support	Skeleton density[c]	ρ_S	1900	$kg/m^3_{skeleton}$
	Dry particle density	ρ_P	760	$kg/m^3_{particle}$
	Wetted particle density	ρ_p	1180	$kg/m^3_{particle}$
	Internal porosity	β_P	60%	$m^3_{void}/m^3_{particle}$
	Tortuosity	τ	≈ 3	-
	Mean Particle diameter	d_P	10	µm

a) Estimated using correlations found in [2].
b) Thermodynamic calculations with PPR78 group contribution using PROSIM software for a flash equilibrium at constant P & T.
c) Commonly taken equal to the graphite density.
d) See for example [3,4] for such typical orders of magnitudes.
e) Calculated from skeleton density and pore volume.
f) See [5] for a discussion about mass transfer inside nanotubes bundles.

S.3.1. G-L external mass transfer

To evaluate the efficiency of the reactor set up to transfer hydrogen in the liquid phase, the mass transfer coefficient ($k_L a_{GL}$) of the reactor has been measured experimentally with a classical physical absorption technique [6, 7] following the H_2 consumption in the regulated and calibrated gas tank. Identical conditions to the experimental ones have been used but without any catalyst (1200 rpm, 80mL of 1M myrcene solution in heptane, 120°C, constant P_{H2} = 20 bar). The H_2 consumption profile of the reserve allowed adjusting and recovering 2 parameters of the system mass balance (eq. S1-S3): the mass transfer coefficient $k_L a_{GL}$ and the final saturation concentration of H_2 in the solution (solubility) C^*_{H2}.

$$dn^L_{H2}(t) = -\,dn^{Res}_{H2}(t) = -\,dp^{res}(t)\frac{V_{res}}{RT_{res}} \qquad \text{(S1)}$$

$$k_L a_{GL} V_R \left(C_{H2}^* - C_{H2}^L(t)\right) = \frac{dn_{H2}^L(t)}{dt} = V_L \frac{dC_{H2}^L(t)}{dt} \quad \text{(S2)}$$

$$-dp^{res}(t) = \frac{RT_{res}}{V_{res}} C_{H2}^* V_L \left(1 - exp\left(-\frac{k_L a_{GL}}{\varepsilon_L} t\right)\right) \quad \text{(S3)}$$

In these equations, $dn_{H2}^L(t)$ is the variation of the quantity of dissolved H_2 in the liquid phase between t_0 and t (mol); $dn_{H2}^{Res}(t)$ is the corresponding variation of H_2 in the calibrated reserve (mol); $dp^{res}(t)$ is the corresponding pressure variation in the reserve (Pa); V_{res} is the volume of the reserve (m^3) ; T_{res} is the temperature of the reserve (K) ; V_L is the liquid volume inside the reactor (m^3) ; ε_L is the liquid fraction inside the reactor (m^3_L/m^3_R) ; C_{H2}^* is the solubility of H_2 in the liquid mixture (mol/m^3); $k_L a_{GL}$ is the G-L mass transfer coefficient (s^{-1}) with $a_{GL}$the specific surface area for G-L mass transfer ($m^2_{GL}/m^3_{Reactor}$).

$k_L a_{GL}$ and C_{H2}^*were estimated as 0.2 s^{-1} and 190 mol_{H2}/m^3_L respectively. The $k_L a_{GL}$ appears typical of well-equipped laboratory stirred tank reactor (for H_2). The experimental solubility is in agreement with the one calculated with the PPR78 thermodynamic model (187 mol/m^3_L).

Based on these mass transfer measurements, a theoretical maximum H_2 consumption, $F_{H2}^{max,GL}$ (in mol_{H2}/s) can be defined for each experiment (S4). This consumption can be linked to the corresponding theoretical apparent reaction rate, $\overline{r_{p,app}^{max}}$ (S5), or to the corresponding theoretical Site Time Yield, STY^{max} (S6), both in full G-L mass transfer regime:

$$F_{H2}^{max,GL} = k_L a_{GL} V_R C_{H2}^* \quad \text{(S4)}$$

$$\overline{r_{p,app}^{max,GL}} = \frac{F_{H2}^{max,GL}}{V_{cata}} = \frac{k_L a_{GL} V_R C_{H2}^*}{V_{cata}} \quad \text{(S5)}$$

$$STY^{max,GL} = \frac{F_{H2}^{max,GL}}{n_{Pd}} = \frac{k_L a_{GL} V_R C_{H2}^*}{n_{Pd}} \quad \text{(S6)}$$

Independently, following the instantaneous consumption curves of H_2, experimental instantaneous apparent reaction rates or STY can be determined at any reaction progress. These latter can be compared to the corresponding theoretical ones to appreciate a fraction of external G-L mass transfer limitation, f_{ex}^{GL} (S7), on the measurements and is analogous of the L-S external mass transfer one because no reaction occurs inside the liquid, only on the catalyst surfaces.

$$f_{ex}^{GL} = \frac{STY}{STY^{max,GL}} = \frac{\overline{r_{p,app}}}{\overline{r_{p,app}^{max}}} \quad \text{(S7)}$$

The relationship between the instantaneous STY and the instantaneous apparent reaction rate $\overline{r_P}$, (per volume of wetted catalyst) is recalled in (S8) :

$$\overline{r_P} = \frac{STY \times \rho_P \times wt.\%_{Pd}}{M_{Pd}} \quad \text{(S8)}$$

Supplementary Table 3 presents this determination for most of the catalysts of the study (those of Figures 1 and 7) at three different reaction progresses: 0.5 $mol_{H2}/mol_{myrcene}$, 2.0 $mol_{H2}/mol_{myrcene}$ and 2.5 $mol_{H2}/mol_{myrcene}$.

Supplementary Table 3: Appraisal of G-L mass transfer limitations.

Catalyst	n_{Pd} (µmol)	STY^{max} ($mol_{H2}/s/mol_{Pd}$)	$STY_{0.5}$ ($mol_{H2}/s/mol_{Pd}$)	$f_{ex,0.5}^{GL}$ (-)	E (-)	$STY_{2.0}$ ($mol_{H2}/s/mol_{Pd}$)	$f_{ex,2.0}^{GL}$ (-)	$STY_{2.5}$ ($mol_{H2}/s/mol_{Pd}$)	$f_{ex,2.5}^{GL}$ (-)
Pd/Al_2O_3	37.6	199	109	55%	1.0	10.2	5%	4.6	2%
Pd/C	36.5	205	168	82%	1.0	72	35%	26	13%
Pd/CNT **also named** $Pd_{2\ SA/NP}/CNT$	38.3	195	144	74%	1.0	44	23%	22	11%
$Pd_{1000\ SA/NP}/CNT$	1.9	3979	184	5%	1.0	1.4	0.04%	N.A.	N.A.
$Pd_{200\ SA/NP}/CNT$	25.0	299	104	35%	1.0	10.4	3%	4.5	2%
$Pd_{40\ SA/NP}/CNT$	25.8	290	544	**187%**	**1.9**	104	19%	50	9%
$Pd_{10\ SA/NP}/CNT$	24.2	308	672	**218%**	**2.2**	272	40%	106	16%

First of all, it is noticeable that the STY^{max} reached different values depending on the different amounts of Pd in each experiment. The $f_{ex,0.5}^{GL}$, for most of the catalysts *(except the $Pd_{1000\_SA/NP}/CNT$ catalyst which contains a very low amount of metal)* is revealed to be high indicating a strong G-L mass transfer impact on the $STY_{0.5}$ measurements and the impossibility to discuss robustly these $STY_{0.5}$. This is indicated in the main text of the article. Interestingly, the 2 more active catalysts present a higher $STY_{0.5}$ compared to the theoretical STY^{max}. This is a phenomenon already observed and explained in stirred tank reactors with very active fine slurry catalyst particles [8, 9]. The approach detailed in [8] is very close to an enhancement factor, E (-), for mass transfer G-L reactive absorption already well established [10]. In the present work, this situation is encountered. Thus, the first points at a reaction progress of 0.5 are used to estimate an experimental E factor as shown in the 6th column of the table. The values are equal to 1 when $f_{ex,0.5}^{GL}$ <100% and equal to the value of $f_{ex,0.5}^{GL}$ when >100%. The values obtained here for the two more active catalysts are consistent with those reported in [8]. For the other reaction progress, accordingly to these measurements, the $F_{H2}^{max,GL}$ (and STY^{max}) takes into account this factor accordingly to (S9):

$$F_{H2}^{max,GL} = Ek_L a_{GL} V_R C_{H2}^* \quad \text{(S9)}$$

For reaction progresses of 2.0 and 2.5 $mol_{H2}/mol_{myrcene}$, the impact of G-L mass transfer on the STY is drastically decreased as shown in the Table and a satisfactory comparison of the observed STY can be drawn on a chemical basis. The Pd_{10SA_NP}/CNT, which is the most active one, is the only catalyst that may still present a possible partial G-L mass transfer hindrance of its intrinsic performance. This partial leveling is a signature of its very high intrinsic activity and does not change the conclusions made in this article. In a quantitative point of view, one can just expect an increase of the observed differences between this catalyst and the other ones.

S.3.2. L-S external mass transfer

In G-L-S slurry reactors, L-S external mass transfer is often less limiting than the G-L one. To verify this common assumption, the classical external mass transfer fraction, f_{ex}^{LS} (defined in S10) has been used for reaction progresses of 0.5, 2.0 and 2.5 $mol_{H2}/mol_{myrcene}$.

$$f_{ex}^{LS} = \frac{\overline{r_P} L}{k_S C_{H2}^*} = \frac{STY}{STY^{max,LS}} \quad \text{with} \quad STY^{max,LS} = \frac{M_{Pd} k_S C_{H2}^*}{\rho_P wt.\%_{Pd} L} \tag{S10}$$

L is the characteristic length of the catalyst (dp/6 for spherical particles) and k_S is the L-S mass transfer coefficient. It has been estimated using the correlation of Armenante & Kirwan [11]. The different results are presented in Supplementary Table 4:

Supplementary Table 4: Appraisal of L-S external mass transfer limitations.

Catalyst	$STY^{max,LS}$ ($mol_{H2}/s/mol_{Pd}$)	$STY_{0.5}$ ($mol_{H2}/s/mol_{Pd}$)	$f_{ex,0.5}^{LS}$ (-)	$STY_{2.0}$ ($mol_{H2}/s/mol_{Pd}$)	$f_{ex,2.0}^{LS}$ (-)	$STY_{2.5}$ ($mol_{H2}/s/mol_{Pd}$)	$f_{ex,2.5}^{LS}$ (-)
Pd/Al_2O_3	137	109	79%	10.2	7.5%	4.6	3.4%
Pd/C	541	168	31%	72	13.3%	26	4.8%
Pd/CNT **also named** $Pd_{2\ SA/NP}$/CNT	31 486	144	0.5%	44	0.1%	22	0.07%
$Pd_{1000\ SA/NP}$/CNT	642 309	184	0.03%	1.4	0.0002%	0.7	0.0001%
$Pd_{200\ SA/NP}$/CNT	48 294	104	0.2%	10.4	0.02%	4.5	0.01%
$Pd_{40\ SA/NP}$/CNT	46 884	544	1.2%	104	0.2%	50	0.1%
$Pd_{10\ SA/NP}$/CNT	49 791	672	1.4%	272	0.6%	106	0.2%

At a reaction progress of 0.5 $mol_{H2}/mol_{myrcene}$, only Pd/Al_2O_3 and Pd/C present a L-S mass transfer limitation. All the CNT catalysts appear free of external L-S mass transfer limitation.

At reaction progress of 2.0 and 2.5 mol/mol, no L-S mass transfer limitation remains at all for all the catalysts (except slightly for the Pd/C) and STY comparisons are consistent and chemically robust.

S.3.3. Internal mass transfer

To evaluate a possible internal mass transfer limitation, the classical Weisz-Prater criterion φ' [12] has been evaluated. When the criterion is inferior to 1 a surface efficiency of 1 is stated. When it is superior to 1, a surface efficiency is approximated as $1/\varphi'$The Supplementary Table 5 presents the results and equations (S11) to (S13), the formula used for .

$$\varphi' = \frac{\overline{r_p} L^2}{D_{eff} C_{H2,su}} \tag{S11}$$

$$D_{eff} = \frac{\beta_P}{\tau} D_{m,H2} \tag{S12}$$

For $\varphi' > 1: \eta_{su} \approx \frac{1}{\varphi'}$ and for $\varphi' < 1: \eta_{su} \approx 1$ (S13)

Supplementary Table 5: Appraisal of possible internal mass transfer limitations.

Catalyst	$Deff\ (m2/s)$	$STY_{2.0}$ **($mol_{H2}/s/mol_{Pd}$)**	φ' **(-)**	η_{su} **(-)**	$STY_{2.5}$ **($mol_{H2}/s/mol_{Pd}$)**	φ' **(-)**	η_{su} **(-)**
Pd/Al_2O_3	$4.0x10^{-10}$	10.2	2.10	≈0.5	4.6	0.95	≈1
Pd/C	$4.0x10^{-10}$	72	1.44	≈0.7	26	0.52	≈1
Pd/CNT **also named** $Pd_{2\ SA/NP}/CNT$	$1.4x10^{-9}$	44	0.004	1	22		1
$Pd_{1000\ SA/NP}/CNT$	$1.4x10^{-9}$	1.4	$1x10^{-5}$	1	0.7		1
$Pd_{200\ SA/NP}/CNT$	$1.4x10^{-9}$	10.4	$6x10^{-4}$	1	4.5		1
$Pd_{40\ SA/NP}/CNT$	$1.4x10^{-9}$	104	$6x10^{-3}$	1	50		1
$Pd_{10\ SA/NP}/CNT$	$1.4x10^{-9}$	272	0.015	1	106		1

All the CNT catalysts at reaction progress 2.0 and 2.5 $mol_{H2}/mol_{myrcene}$ are free of internal limitations. This remains true for the reference Pd/Al_2O_3 and Pd/C at the reaction progress of 2.5 $mol_{H2}/mol_{myrcene}$. For these catalysts, an intermediate regime with little mass transfer resistance may be present at a reaction progress of 2.0 $mol_{H2}/mol_{myrcene}$ because $1 < \varphi' < 3$. This is due to the bigger size of the catalyst particles.

S.3.4. Global conclusion on mass transfer limitations

Due to the high reactivity of the terminal alkene and the conjugated double bond of myrcene, the first hydrogenation is very fast and the overall hydrogenation of this study is subject to external mass transfer limitations (either G-L, L-S or both) at low reaction progress (typically < 1.0 $mol_{H2}/mol_{myrcene}$). For the usual reference hydrogenation catalysts (Pd/Al_2O_3 and Pd/C), at higher reaction progress, (2 or 2.5 $mol_{H2}/mol_{myrcene}$), most of the experimental instantaneous STY measurements are free of external or internal limitations. Only the most active catalysts ($Pd_{40\_SA/NP}/CNT$ and $Pd_{10\_SA/NP}/CNT$) can be subject to a little G-L limitation that may hinder slightly their true performance.

Regarding internal mass transfer limitations, only Pd/Al_2O_3 and Pd/C may be subject to a little hindrance of their true kinetics at a reaction progress of 2.0 $mol_{H2}/mol_{myrcene}$. This latter tends to disappear at a reaction progress of 2.5 $mol_{H2}/mol_{myrcene}$.

Overall, comparison of instantaneous STY of this study is allowed and consistent for reaction progresses higher than 2.0. The conclusions drawn in this paper can be linked with chemical phenomena.

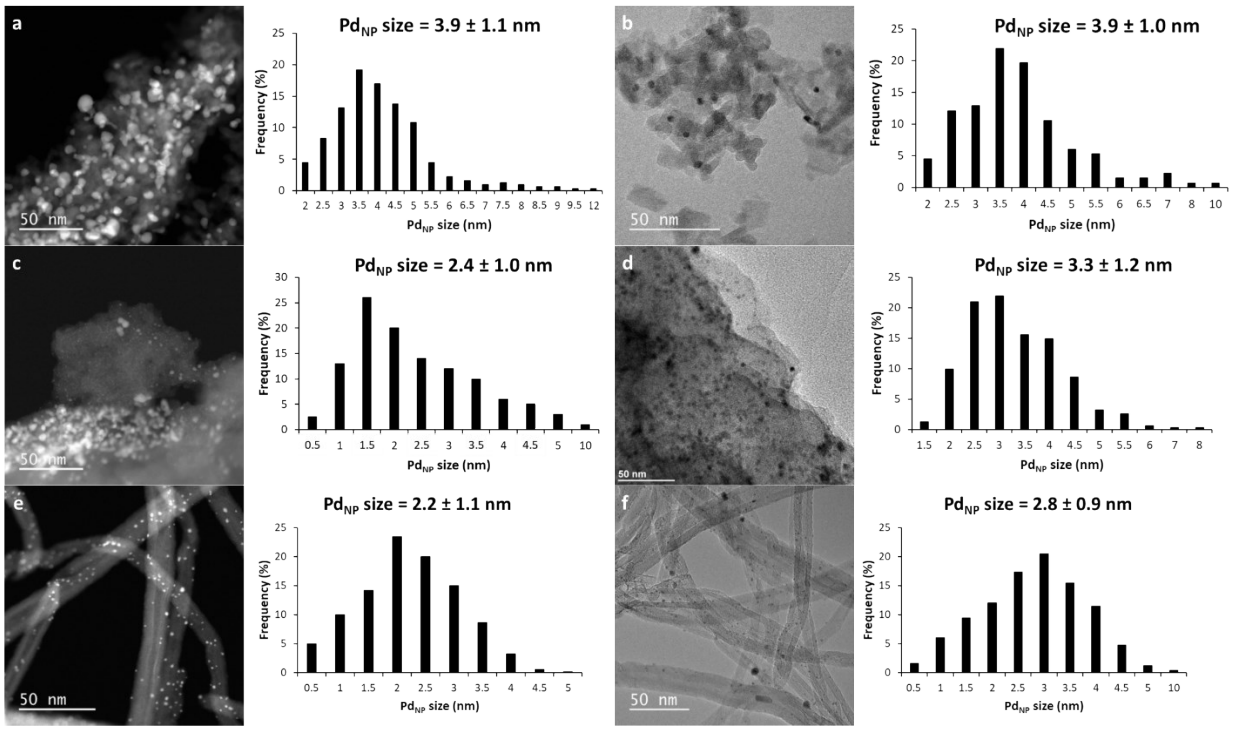

Fig. S1. STEM-HAADF and TEM micrographs, and histograms of Pd_{NP} sizes of: **a** fresh Pd/Al_2O_3; **b** Pd/Al_2O_3 after β-myrcene hydrogenation; **c** fresh Pd/C; **d** Pd/C after β-myrcene hydrogenation; **e** fresh Pd/CNT; and **f** Pd/CNT after *β*-myrcene hydrogenation. Scale bar = 50 nm.

Fig. S2. Photo of the metallic foam coated in the tubular reactor for catalyst stability study under continuous reactor operation.

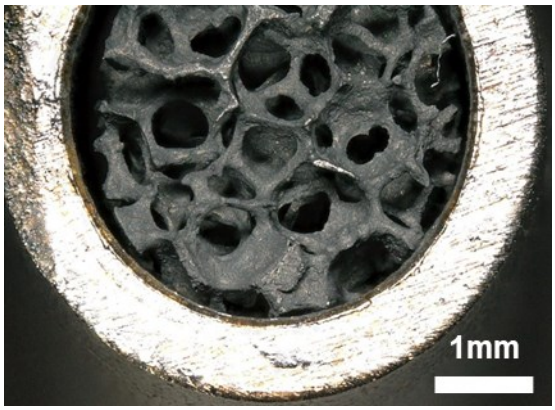

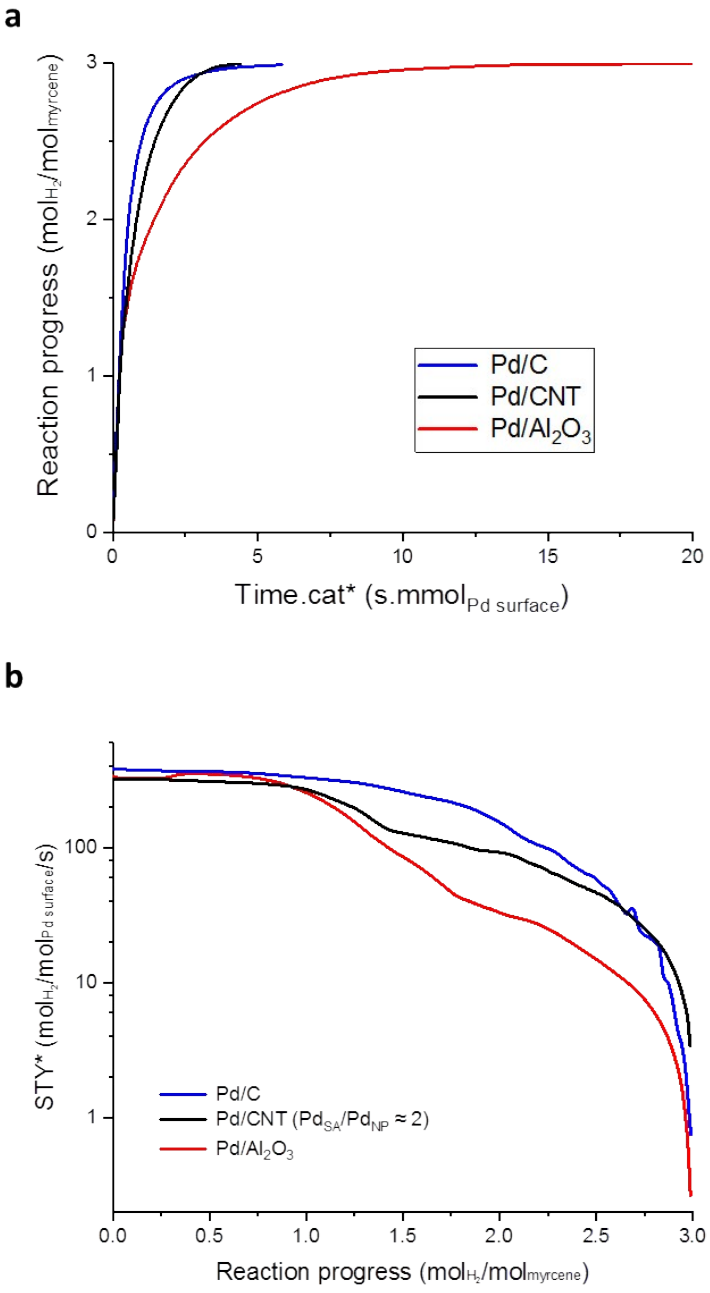

Fig. S3. Catalytic results on Pd/Al_2O_3, Pd/C and $Pd_{2\_SA/NP}$/CNT as a function of surface Pd. β-myrcene hydrogenation reaction. The reaction was carried out over supported Pd catalysts. P_{H2} = 20 bar - T = 120°C - myrcene 1 M (80 mL) - solvent heptane - 200 mg cat. **a** Reaction progress as a function of time.cat*. **b** STY* as a function of reaction progress.

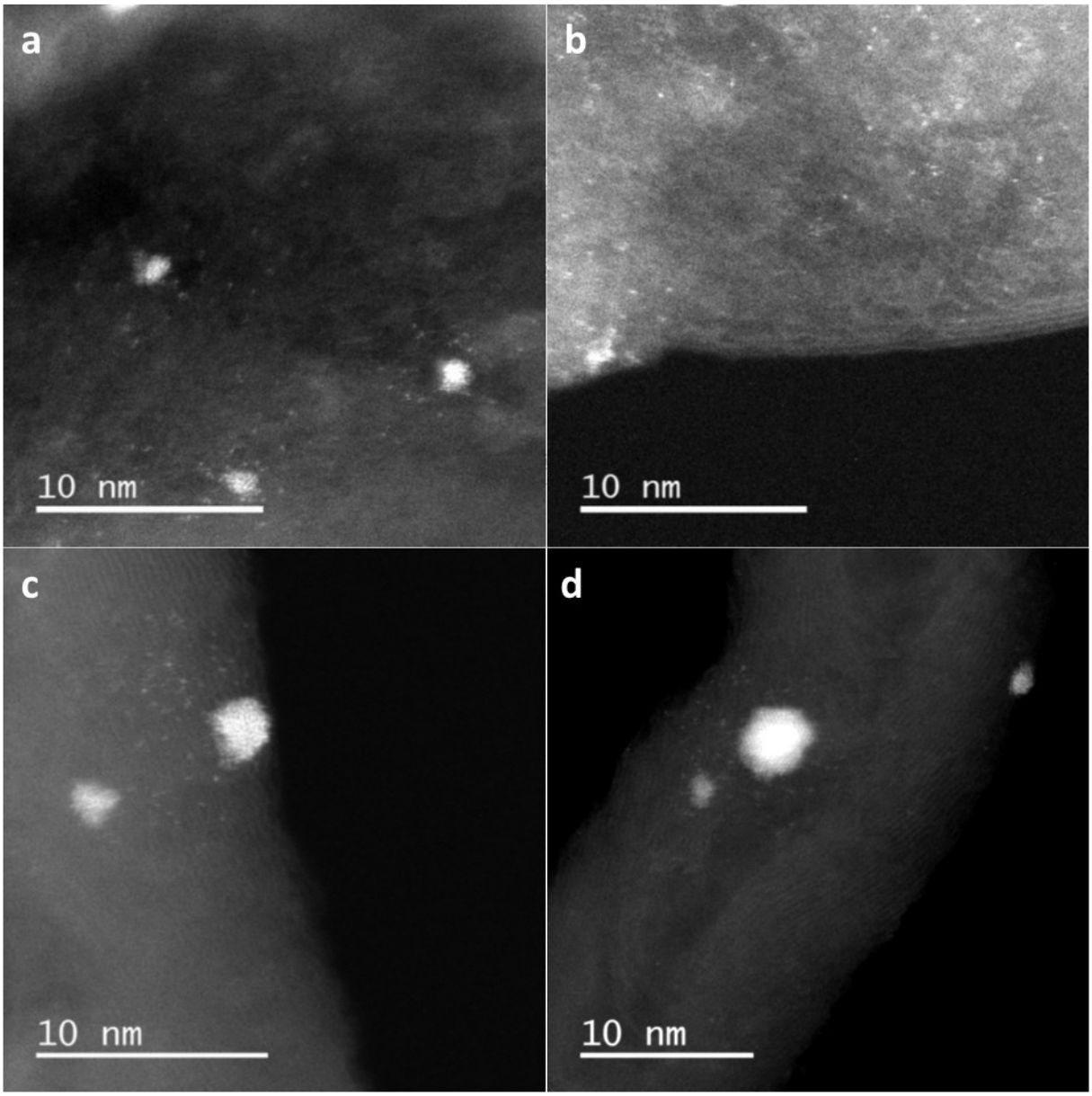

Fig. S4. STEM-HAADF images of **a** and **b** Pd/FLG (FLG = few layer graphene); and **c** and **d** Pd/CNF (CNF = carbon nanofibers), showing the coexistence of Pd_{SA} and Pd_{NP}.

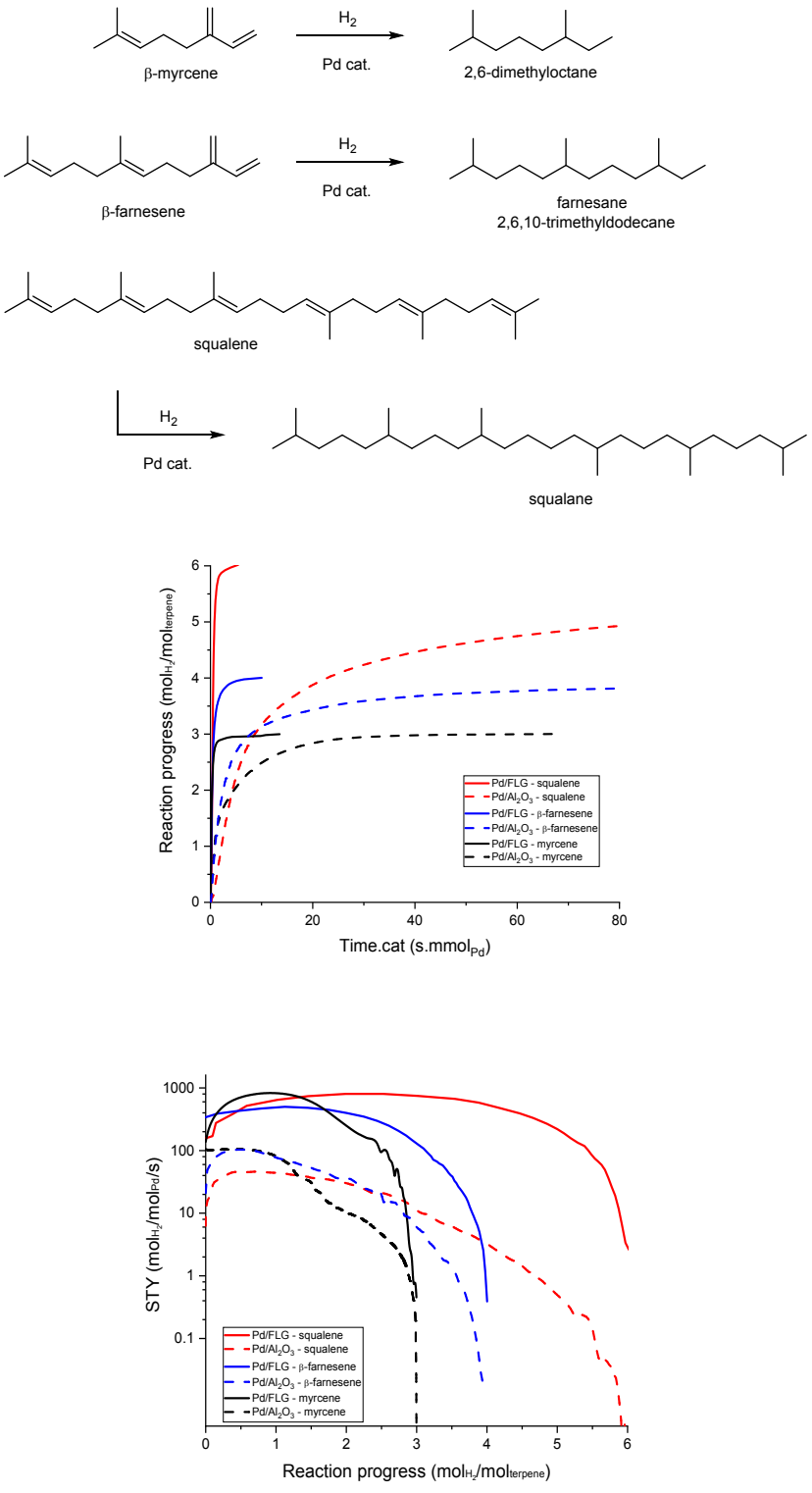

Fig. S5. Comparison of the catalytic performances of Pd/Al_2O_3 and Pd/FLG for the total hydrogenation of myrcene, farnesene and squalene. Hydrogenation reactions carried out over supported Pd catalysts. PH_2 = 20 bar - T = 120°C - substrate 1 M (80 mL) - solvent heptane - 280 mg cat.

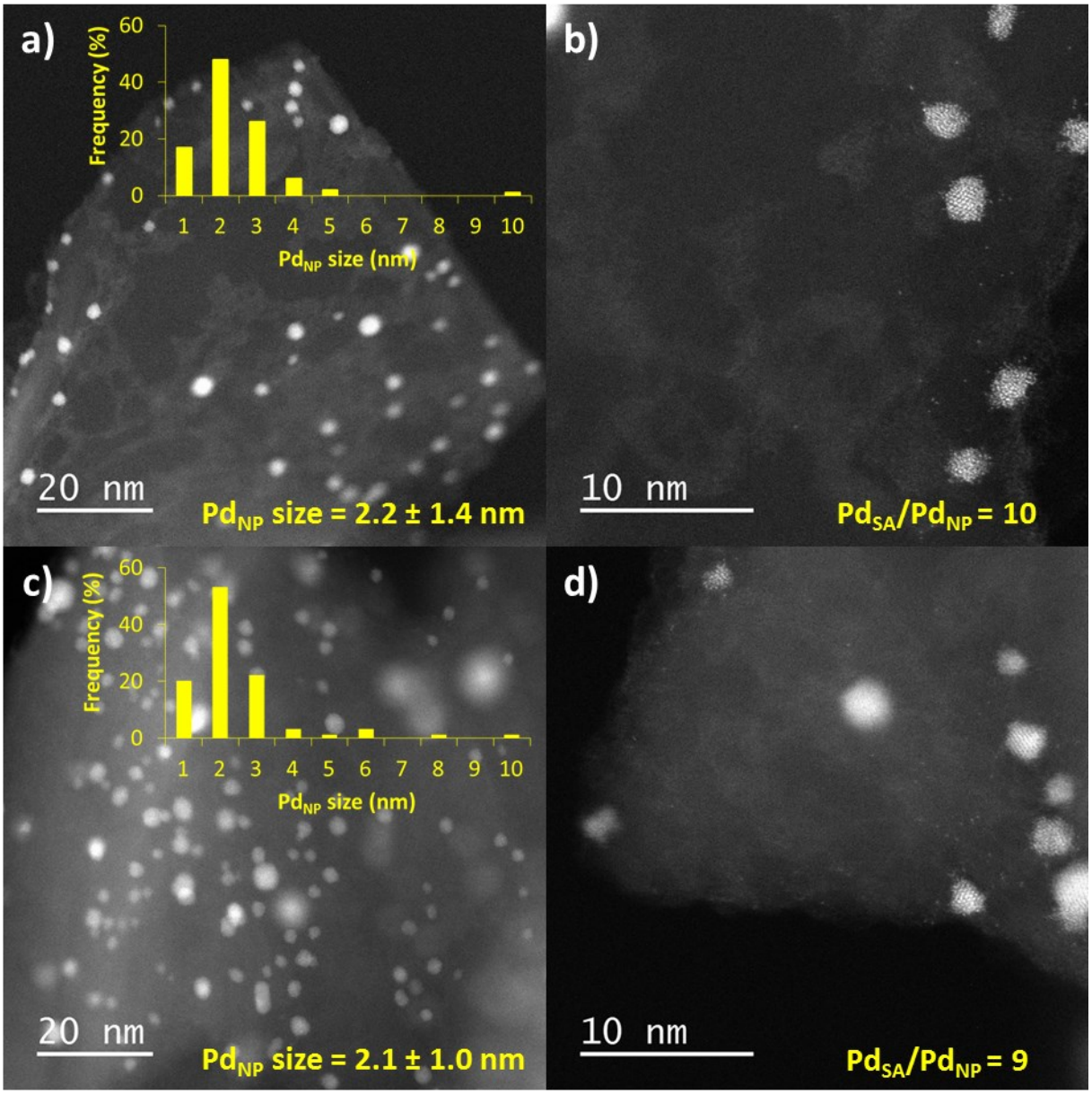

Fig. S6. STEM-HAADF micrographs, particle size distribution and Pd_{SA}/Pd_{NP} ratio for the Pd/FLG catalyst: a) and b) before catalysis; and c) and d) after myrcene hydrogenation.

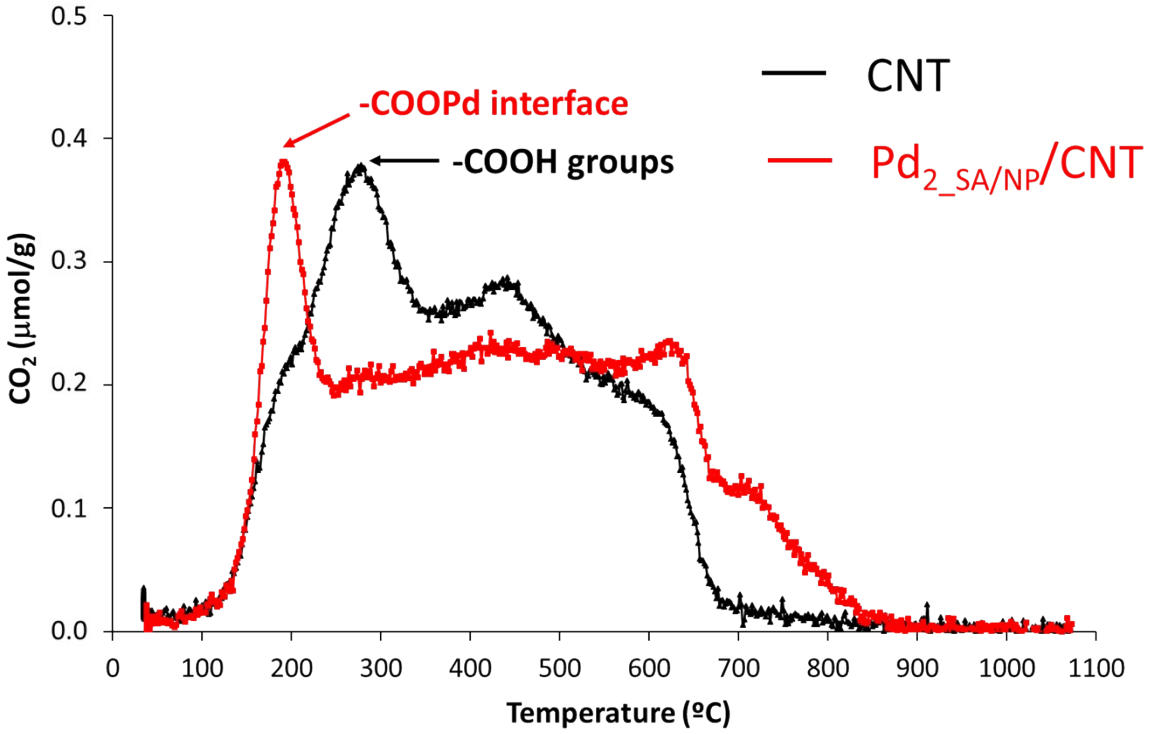

Fig. S7. CO_2 TPD profiles of the CNT support and the $Pd_{2\_SA/NP}$/CNT catalyst showing the disappearance of most of the surface carboxylic groups after catalyst preparation, and the appearance of a Pd-OOC- interface.

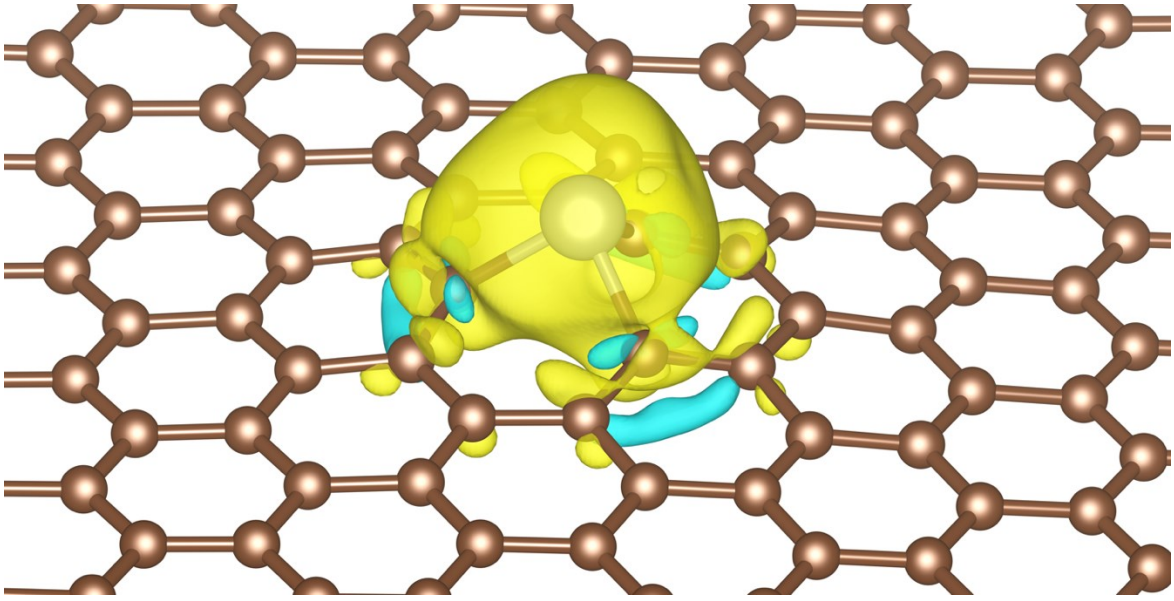

Fig. S8. Isosurface plot of the electronic density differences ($\Delta\rho = \rho_{Pd-SAC} - \rho_{Pd} - \rho_{SAC}$) for negative (in cyan) and positive (in yellow) isovalue of 0.002 e^-/Å. The charge transfer from Pd SA *4d* orbitals to the defective (single vacancy in graphene) support is estimated to be 0.37 e^-.

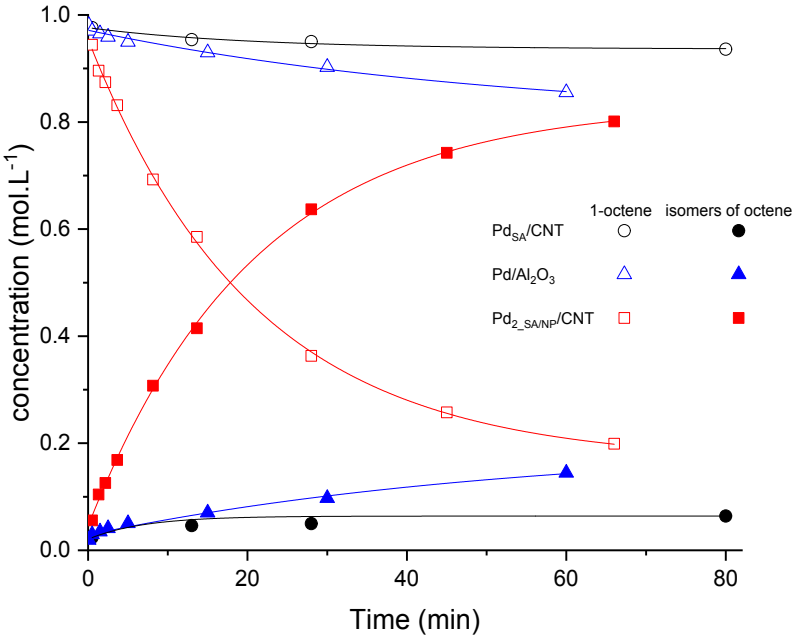

Fig. S9. Evolution of the composition of the solution during 1-octene H_2-assisted isomerization as the function of time and catalysts Pd_{SA}/CNT, Pd/Al_2O_3 and $Pd_{2\_SA/NP}$/CNT. Reaction conditions: 1-octene (1M) in heptane, Pd 0.4 mg (60 ppm), reflux (98 °C), H_2 1 atm. In the case of the CNT catalyst no measurable activity was noticed.

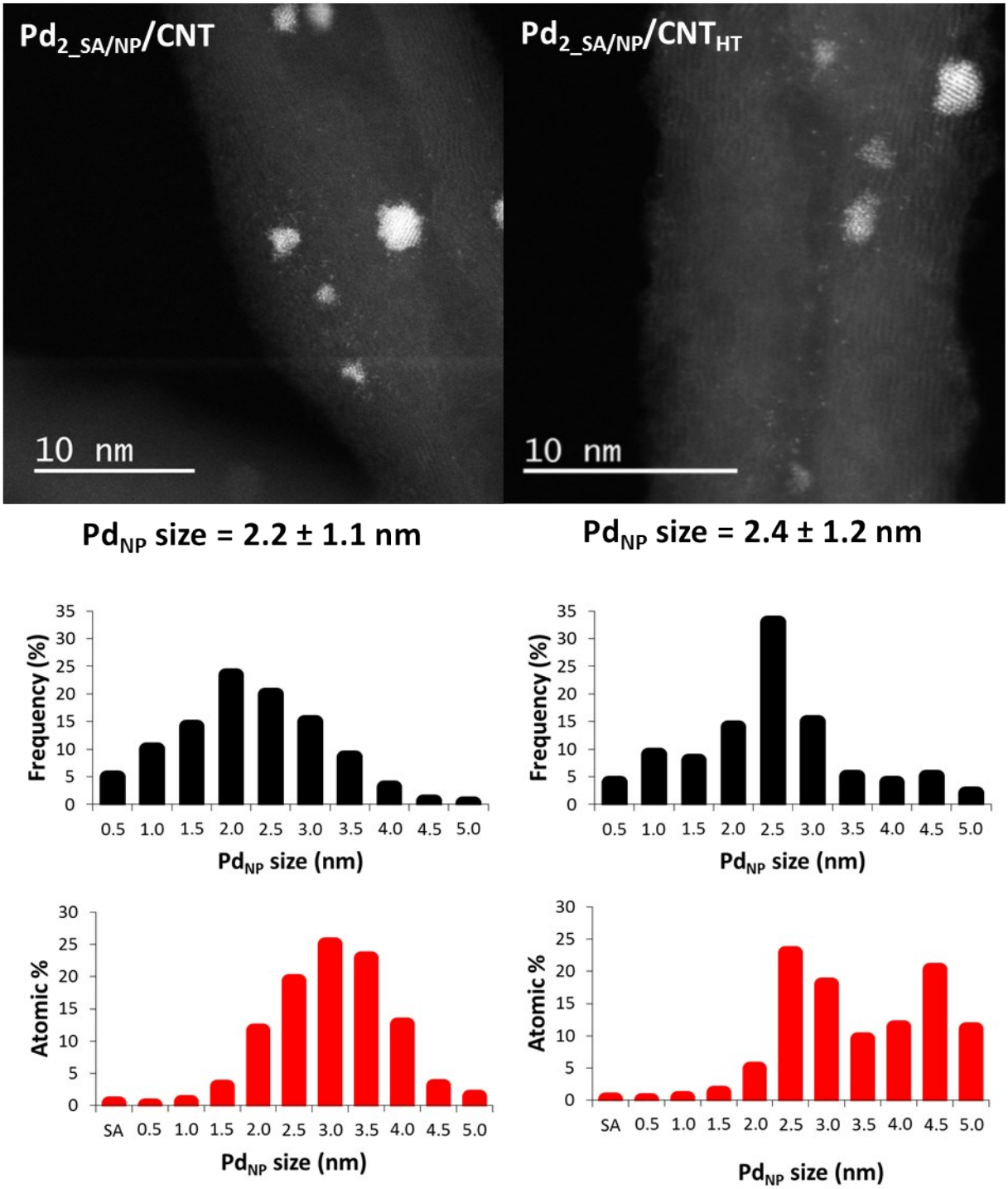

Fig. S10. STEM-HAADF micrographs of $Pd_{2\_SA/NP}/CNT$ and $Pd_{2\_SA/NP}/CNT_{HT}$ catalysts and related particle size distribution based on total particles and on total atoms.

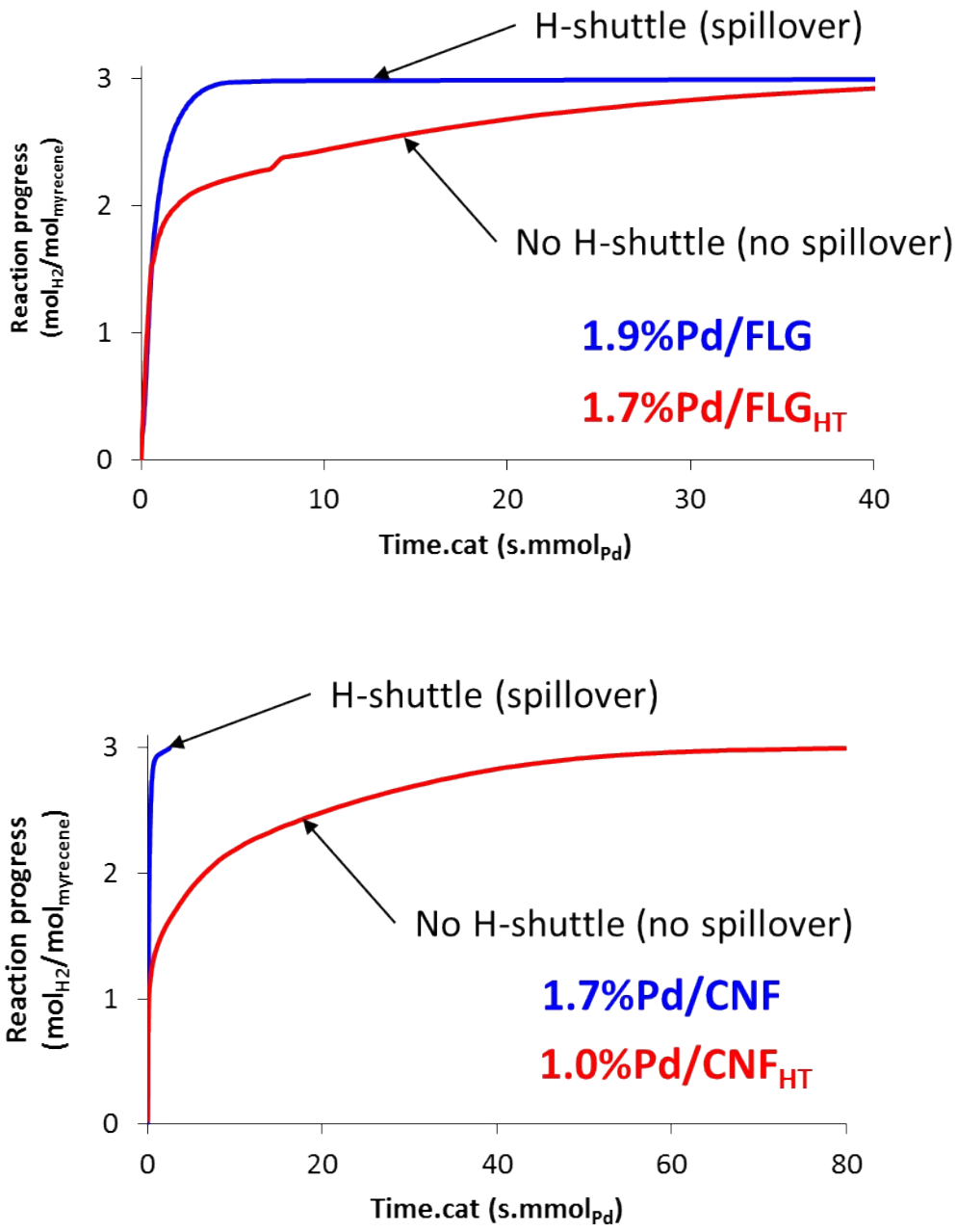

Fig. S11. *β*-Myrcene hydrogenation reactions carried out over Pd/FLG, Pd/FLG$_{HT}$, Pd/CNF and Pd/CNF$_{HT}$ catalysts. P_{H2} = 20 bar - T = 120°C - *β*-myrcene 1 M (80 mL) – solvent heptane - 200 mg cat.

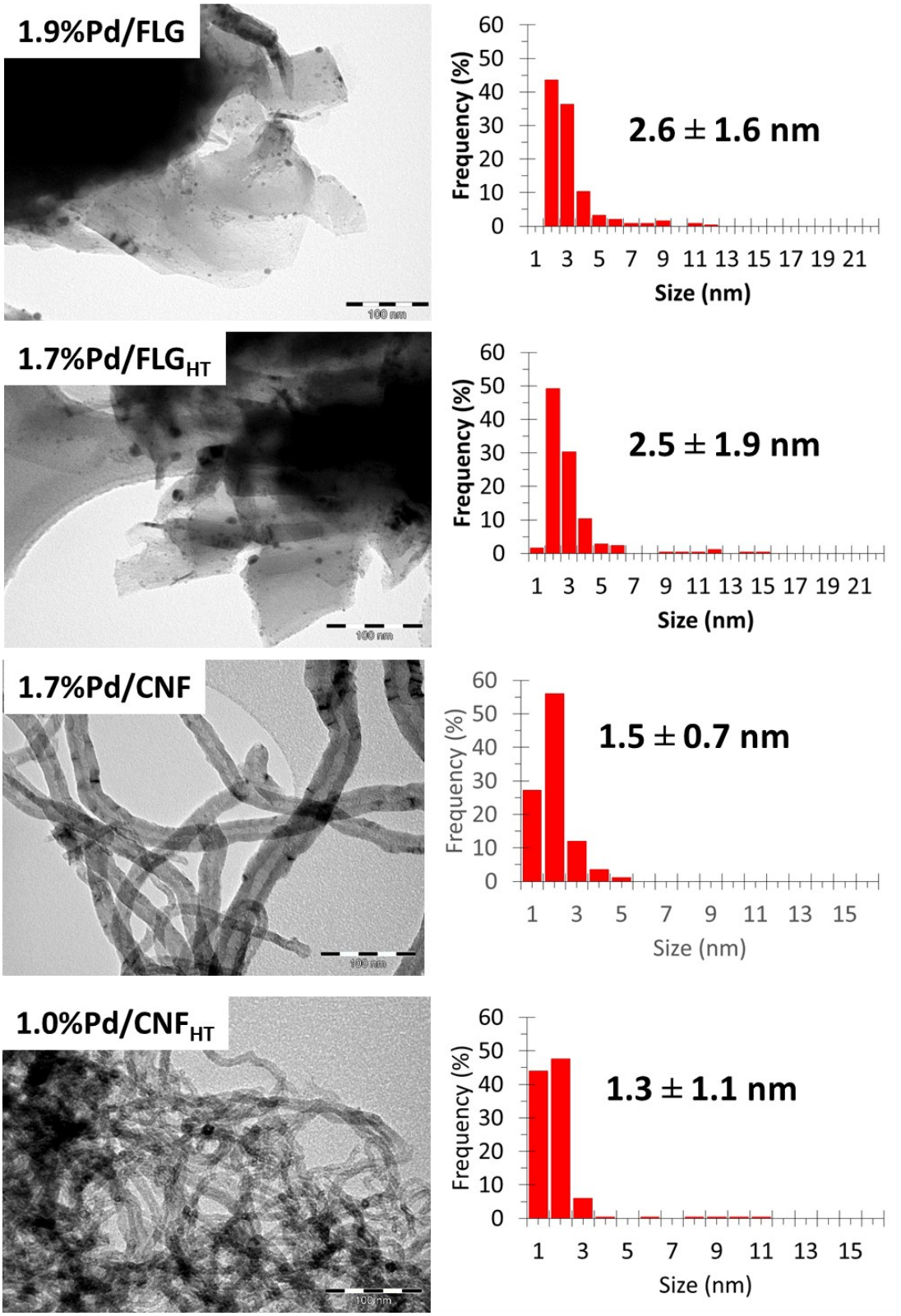

Fig. S12. TEM micrographs and particle size distribution of 1.9%Pd/FLG, 1.7%Pd/FLG$_{HT}$, 1.7%Pd/CNF and 1.0%Pd/CNF$_{HT}$ catalysts.

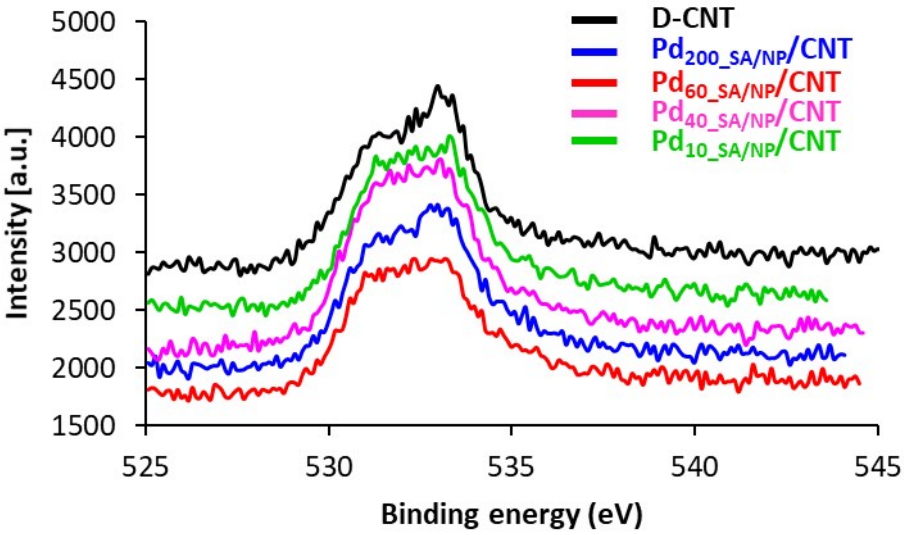

Fig. S13. O 1*s* XPS spectra of $Pd_{200\_SA/NP}$/CNT, $Pd_{60\_SA/NP}$/CNT, $Pd_{40\_SA/NP}$/CNT, $Pd_{10\_SA/NP}$/CNT and D-CNT.

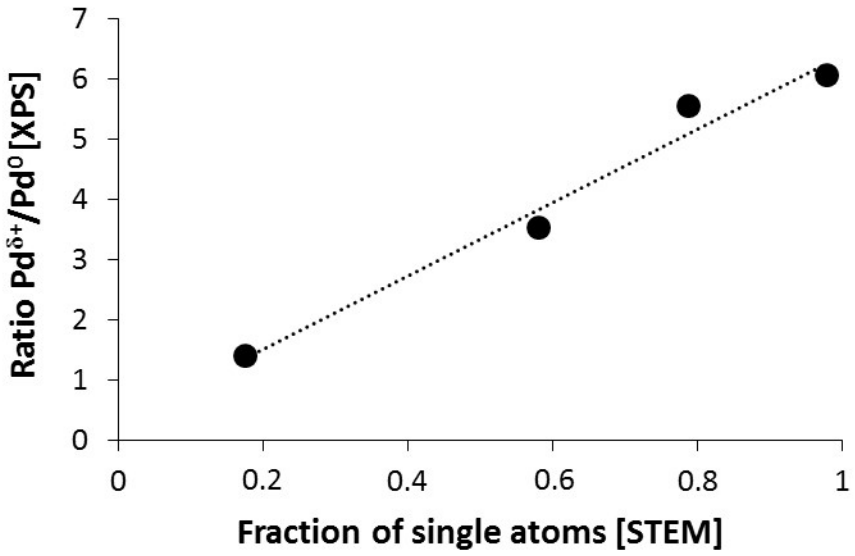

Fig. S14. Correlation between the ratio $Pd^0/Pd^{\delta+}$ determined by XPS and the fraction of SA in the same samples determined from STEM.

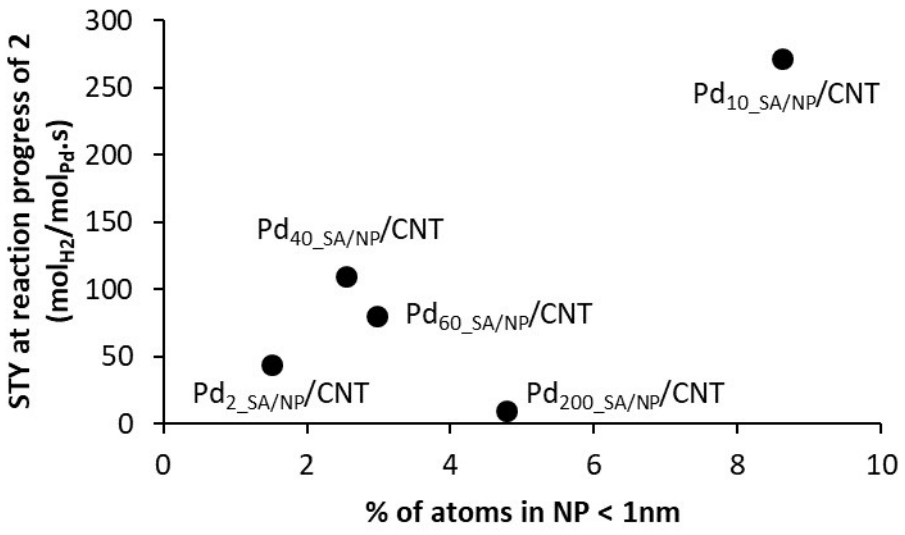

Fig. S15. Correlation between the the percentage of atoms present in clusters (NP < 1nm) and the measured STY at a reaction progress of 2.

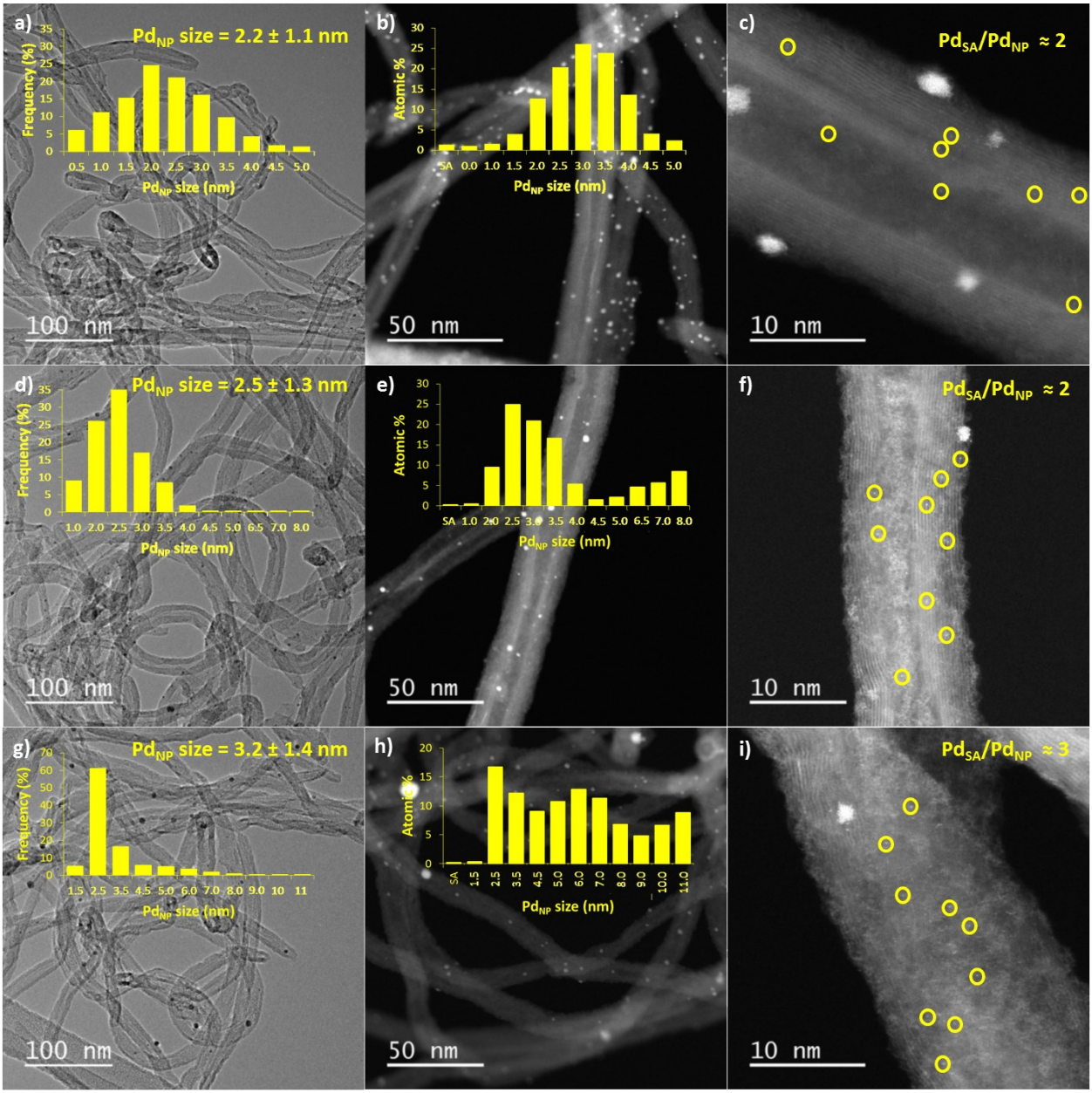

Fig. S16. TEM and STEM micrographs and particle size distribution based on total particles and on total atoms for: a) to c) $Pd_{2\_SA/NP}$/CNT; d) to f) $Pd_{2\_SA/NP}$/CNT coated on metallic open-cell solid foam cylinders before catalysis; and g) to i) $Pd_{2\_SA/NP}$/CNT coated on metallic open-cell solid foam cylinders after catalysis.

Additional references

1. A. Borodzinski, M. Bonarowska, Relation between crystallite size and dispersion on supported metal catalysts, Langmuir, 13 (1997) 5613-5620.
2. R. C. Reid, J. M. Prausnitz, B. E. Poling, The properties of gases and liquids 4th edition, McGraw-Hill Inc. New York (1987).
3. E. Lam, J. H. T. Luong, Carbon materials as catalyst supports and catalysts in the transformation of biomass to fuels and chemicals. ACS Catal. 4 (2014) 3393-3410.
4. S. Jin, W. Qian, Y. Liu, F. Wei, D. Wang, J. Zhang. Granulated carbon nanotubes as the catalyst support for Pt for the hydrogenation of nitrobenzene. Aust. J. Chem. 63 (2010) 131-134.
5. P. W. A. M. Wenmakers, J. van der Schaaf, B. F. M. Kuster, J. C. Schouten. ‘‘Hairy Foam’’: carbon nanofibers grown on solid carbon foam. A fully accessible, high surface area, graphitic catalyst support. J. Mater. Chem., 18 (2008) 2426-2436.
6. R. V.Chaudhari, R. V. Gholap, G. Emig, H. Hofman. Gas-Liquid mass transfer in dead-end autoclave reactors. Can.J. Chem. Eng. 65 (1987) 744-751.
7. E. Dietrich, C. Mathieu, H. Delmas, J. Jenck. Raney-Nickel catalyzed hydrogenations: gas-liquid mass transfer in gas-induced stirred slurry reactors. Chem. Eng. Sci. 47 (1992) 3597-3604.
8. Z. Junmei, X. Chunjian, Z. Ming. The mechanism model of gas-liquid mass transfer enhancement by fine catalyst particles. Chem. Eng. J. 120 (2006) 149-156.
9. S. Karve, V.A. Juvekar. Gas absorption into slurries containing fine catalyst particles. Chem. Eng. Sci. 45 (1990) 587-594.
10. G. F. Froment, K. B. Bischoff. Chemical Reactor Analysis and Design. Wiley, New York (1990).
11. P. M. Armenante, D. J. Kirwan. Mass transfer to microparticles in agitated systems. Chem. Eng. Sci. 44 (1989) 2781-2796.
12. P.B. Weisz, C.D. Prater. Interpretation of measurements in experimental catalysis, in: Adv. Catal., Elsevier, 1954: pp. 143–196